1.32 Design and Components of Photovoltaic Systems

WGJHM van Sark, Utrecht University, Utrecht, The Netherlands

1.32.1 Introduction

In general, two types of photovoltaic (PV) solar energy systems exist: grid-connected and stand-alone (**Figure 1**). Grid-connected PV systems consist of one or more PV modules, one or several inverters to convert direct current (DC) PV power into alternating current (AC), cabling, and a mounting structure and are connected to the conventional electricity grid via the inverter [1]. Grid-connected PV system sizes range from ~50 Wp (one module) via small scale (0.5–4 kWp) for private homeowners, to medium scale (4–100 kWp), to large scale (0.1–100 MWp), while very large scale PV (VLS-PV) systems may range above 1 GWp [2]. Additional components to the modules that together form a PV system are denoted balance of system (BOS) components.

Stand-alone systems consist of one or a few PV modules, a battery for electrical storage, cabling, mounting structure, and a charge controller. As the output of the PV panel varies with the solar intensity and temperature, the charge controller is needed to condition the DC output and deliver it to the batteries. Stand-alone systems are usually designed to meet a specific load, for instance in solar home systems (SHSs); a few modules provide power to charge a battery during the day, and some lighting appliances and radio or television set can be powered in the evening [3]. Other applications are rural central power plants (mini grids), power supply for communication, lighting, cathodic protection, water pumps, and buoys.

PV modules or panels are built from several solar cells and range from about 0.024 (1 crystalline silicon cell of $156 \times 156\ mm^2$) to $2\ m^2$ in size, depending on the application possibilities and marketability as judged by various manufacturers. Building-integrated PV (BIPV) and power plant applications usually require the larger size, whereas for rural electrification projects, the smaller size suffices. The rated power, that is, the power generated by the PV module under standard test conditions (STCs) of $1000\ W\ m^{-2}$ solar intensity at air mass (AM) 1.5 global spectrum and 25 °C module temperature, depends on the area of the module and is usually denoted as Watt-peak or Wp. At 15% efficiency, typical rated powers range from 3.65 ($0.024\ m^2$) to 350 Wp ($2\ m^2$). Panels are usually connected to form a solar array, to reach typical sizes of 3–4 kWp for individual houses.

System performance depends on the conversion efficiency of all components, of which the PV module has the most influence. For both PV modules and inverters, efficiency curves as a function of irradiance should be used to determine the efficiency of the whole system, while other losses should also be taken into account. For system design purposes, that is, to estimate the annual

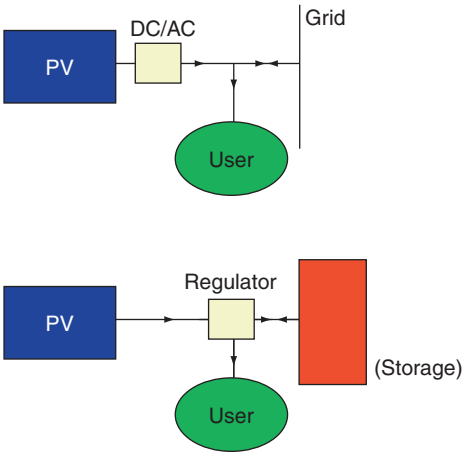

Figure 1 Grid-connected (top) and stand-alone (bottom) PV systems.

amount of generated energy per installed capacity, irradiation and temperature data are needed on an hourly basis. By convoluting these data sets with efficiency curves for modules and inverters, one can determine the expected annual yield.

In the following, panels and BOS components are discussed, with a focus on the performance of cells and modules; various loss factors in grid-connected systems are briefly described. Finally, two case studies that illustrate PV system design will be presented: a hybrid system on the Maldivian island Mandhoo and a large system in Abu Dhabi.

1.32.2 PV Cells and Modules

1.32.2.1 Solar Cells

The performance of a solar cell, the building block of solar panels, is characterized by four general parameters [4], which are derived from the current–voltage characteristic (I–V) measured under STCs, see also **Figure 2**: open-circuit voltage V_{oc}, short-circuit current I_{sc}, fill factor FF, and energy conversion efficiency η. The latter is calculated from

$$\eta = \frac{P_{max}}{AP_{in}} = \frac{V_{mpp}I_{mpp}}{AP_{in}} = \frac{V_{oc}I_{sc}FF}{AP_{in}} \quad [1]$$

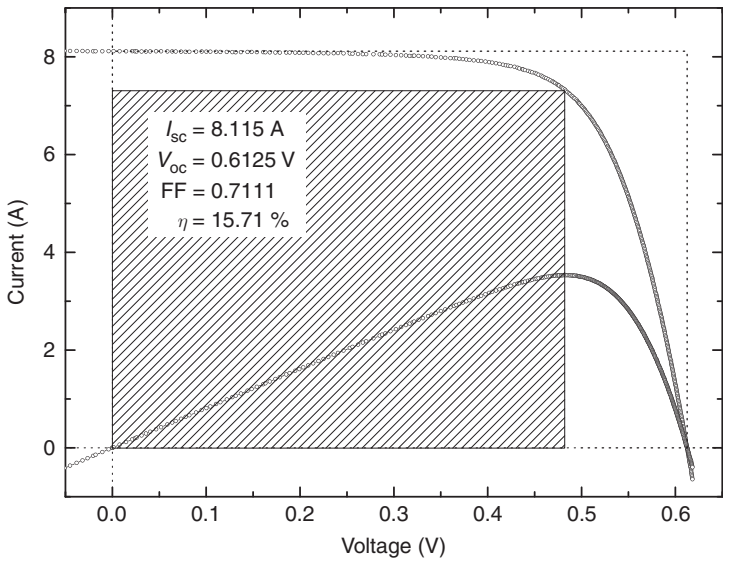

Figure 2 I–V characteristics of a 156 × 156 mm^2 crystalline silicon solar cell measured at STC. Performance parameters are I_{sc} = 8.115 A; V_{oc} = 0.6125 V, and η = 15.71%. The fill factor is a measure of the squareness of the I–V characteristics and is defined as FF = $V_{mpp}I_{mpp}/V_{oc}I_{sc}$ and equals FF = 0.7111. In other words, 71.11% of the area (0.0) to (V_{oc}, I_{sc}) is filled. From van Sark WGJHM (2007) Teaching the relation between solar cell efficiency and annual energy yield. *European Journal of Physics* 28: 415–427 [5].

where P_{max} is the maximum generated power, A the cell area, and P_{in} the incident power (=1000 W m^{-2} at STC). The maximum power P_{max} is given by $P_{max} = V_{mpp}I_{mpp}$, where V_{mpp} and I_{mpp} are the voltage and current, respectively, at the maximum power point (MPP). The fill factor is thus defined as $FF = V_{mpp}I_{mpp}/V_{oc}I_{sc}$.

In order to make an estimate of the irradiation dependence of the efficiency, van Sark has developed a method [5] (see also below) starting with the general expression for the current–voltage characteristic, which reflects the fact that a solar cell is a single-junction diode [4]:

$$I = I_L - I_{01}\left(\exp\frac{qV'}{kT} - 1\right) - I_{0n}\left(\exp\frac{qV'}{nkT} - 1\right) - \frac{V'}{R_{sh}}$$
$$V' = V + IR_{se} \qquad [2]$$

in which I_L is the photocurrent, I_{01} and I_{0n} are diode saturation currents for the diodes with ideality factor 1 and n, respectively, V' is the effective voltage, R_{se} and R_{sh} represent series and parallel (shunt) resistances, respectively, k is Boltzmann's constant (1.38×10^{-23} J K^{-1}), T is the temperature (K), and q is the elementary charge (1.602×10^{-19} C). At room temperature, kT/q equals 25.67 mV and is also denoted as the thermal voltage V_{th}.

For an ideal single junction, eqn [2] is simplified to include one diode (with $n = 1$), zero series resistance, and infinite shunt resistance. Then, V_{oc} and I_{sc} are given by

$$V_{oc} = \frac{kT}{q}\ln\left(\frac{I_L}{I_0} + 1\right)$$
$$I_{sc} = I_L \qquad [3]$$

Normal operating conditions of PV systems are rarely STC. Depending on geographical location, season, and time of the day, full sun conditions or (partly) overcast skies will prevail. Incident spectra also differ as a function of longitude and time of day from AM1 to about AM10. Under full sun, the temperature of the module can be much larger than 25 °C, reaching values between 60 and 80 °C. This lowers the efficiency, as the open-circuit voltage and, to a lesser extent, the fill factor are dependent on temperature. This is usually parameterized by the use of temperature coefficients dV_{oc}/dT and dFF/dT. The values differ for different solar cell materials, but in general are negative. A small positive temperature coefficient dJ_{sc}/dT of the short-circuit current may be present.

Lower irradiances not only lower the power output of the solar cell (**Figure 3**) but also affect its efficiency, depending on series resistance. Many cells with appreciable series resistance show a maximum efficiency at irradiances lower than 1000 W m^{-2}, peaking between 100 and 500 W m^{-2} [6]; see also **Figure 4**. A shunt resistance has an influence especially at irradiances < 100 W m^{-2} [7]. If indoor irradiation conditions prevail (≪ 100 W m^{-2}), the performance drop will be much more dramatic. In case measured I–V curves as in **Figure 3** are not available, a simple STC method to calculate irradiance-dependent efficiencies for cells with high shunt values can be used, which was developed by van Sark *et al.* [5, 8, 9].

1.32.2.1.1 Irradiance-dependent solar cell performance

1.32.2.1.1(i) Empirical three-parameter method

When I–V characteristics are available that have been measured at irradiance values other than STC, it is possible to fit the parameters of an empirical-derived relation between efficiency and irradiance. **Figure 3** shows I–V characteristics of a crystalline

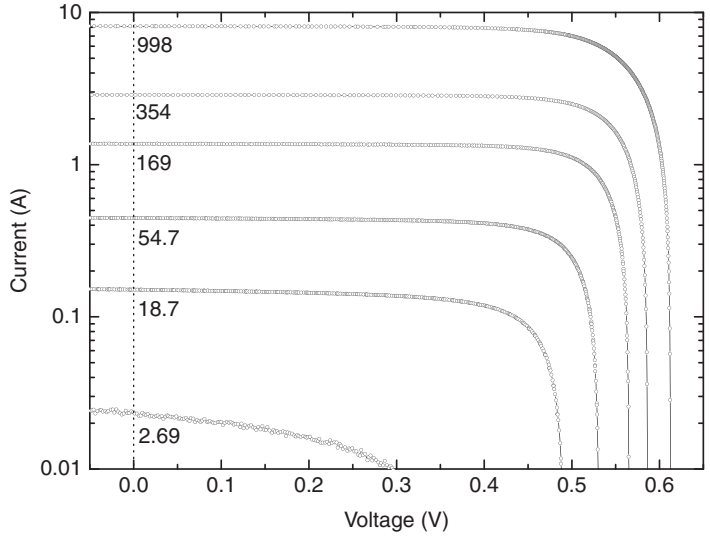

Figure 3 I–V characteristics of a 156 × 156 mm^2 solar cell measured at various irradiance values, that is, 2.69, 18.7, 54.7, 169, 354, and 998 W m^{-2}. From van Sark WGJHM (2007) Teaching the relation between solar cell efficiency and annual energy yield. *European Journal of Physics* 28: 415–427 [5].

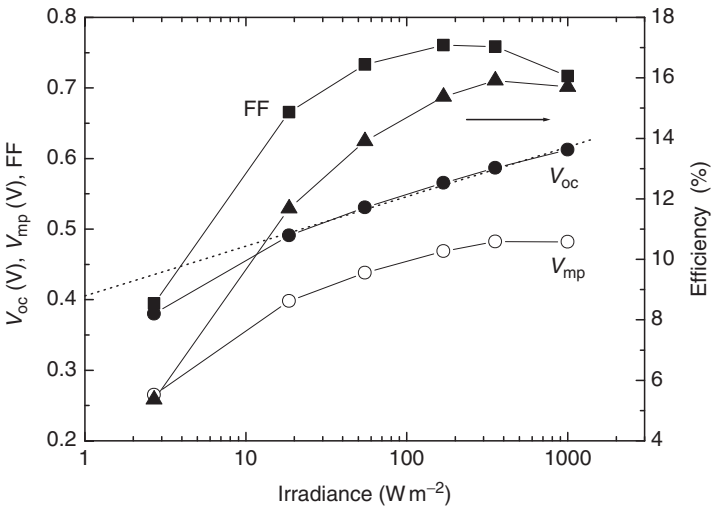

Figure 4 Performance parameters as a function of irradiance, derived from the data in **Figure 2**. The dotted line illustrates a single logarithmic dependence of the open-circuit voltage. From van Sark WGJHM (2007) Teaching the relation between solar cell efficiency and annual energy yield. *European Journal of Physics* 28: 415–427 [5].

silicon (c-Si) cell for various irradiance values. The efficiency values determined from these curves are fitted using a three-parameter equation proposed by Beyer *et al.* [10]:

$$\eta(G) = a_1 + a_2 G + a_3 \ln(G) \quad [4]$$

Figure 5 shows the fit results, the parameters are $a_1 = 0.214 \pm 0.004$, $a_2 = -0.060 \pm 0.007$, and $a_3 = 0.0265 \pm 0.0010$, when G is taken in kW m^{-2}. The parameters for another cell made from multicrystalline silicon (mc-Si) are $a_1 = 0.197 \pm 0.004$, $a_2 = -0.051 \pm 0.006$, and $a_3 = 0.0269 \pm 0.0011$.

During analysis, however, it was found that at very low irradiance intensities, negative efficiencies can also result using eqn [4]. Therefore, Reich *et al.* modified the original phenomenological equation by including another parameter (a_4) in the logarithmic part to avoid negative efficiencies and improve fitting accuracy at low (< 1 W m^{-2}) light intensities [8] that prevail indoors [9]:

$$\eta(G) = a_1 + a_2 G + a_3 \ln(a_4 + G) \quad [5]$$

For outdoor energy yield determination, the three-parameter eqn [4] suffices.

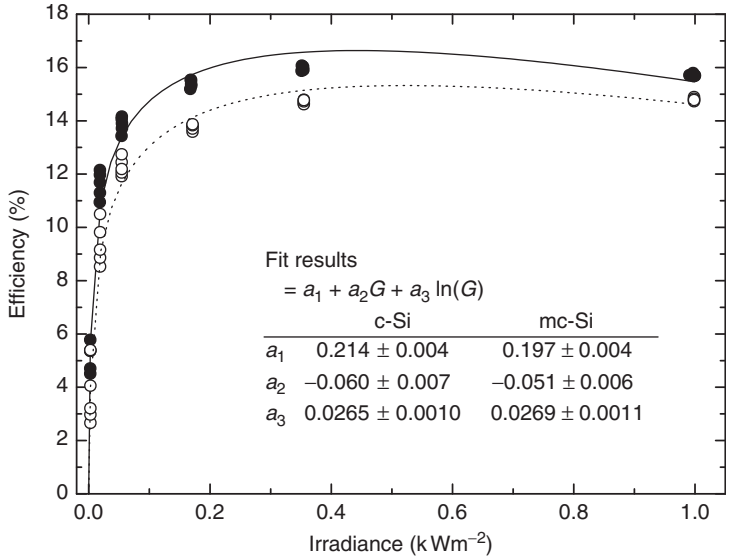

Figure 5 Measured efficiencies of c-Si and mc-Si solar cells as a function of irradiance. For c-Si, the fit shows a maximum efficiency of 16.64% at 0.45 kW m^{-2}, while the measured efficiency at 1 kW m^{-2} (STC) is 15.47%. For mc-Si, the fit shows a maximum efficiency of 15.32% at 0.525 kW m^{-2}, while the measured efficiency at 1 kW m^{-2} (STC) is 14.80%. From van Sark WGJHM (2007) Teaching the relation between solar cell efficiency and annual energy yield. *European Journal of Physics* 28: 415–427 [5].

1.32.2.1.1(ii) STC method

In order to make an estimate of the irradiation dependence of the efficiency, the simplified expression for the current–voltage characteristic, eqn [3], is used as the starting point. Green has derived an empirical relation between fill factor FF_0 and normalized open-circuit voltage v_{oc}, defined as $v_{oc} = V_{oc}(q/kT)$, for zero series resistance and infinite shunt resistance [4]:

$$FF_0 = \frac{v_{oc} - \ln(v_{oc} + 0.72)}{v_{oc} + 1} \quad [6]$$

Fill factor loss due to series resistance R_s can then be represented by

$$FF = FF_0(1 - r_s) \quad [7]$$

where r_s is the normalized series resistance given as $r_s = R_s/R_{CH}$. The characteristic resistance R_{CH} is defined as $R_{CH} = V_{oc}/I_{sc}$.

Equations [6] and [7] have been thoroughly validated and are found to be accurate for $v_{oc} > 10$ and $r_s < 0.4$ [4].

Similarly, shunt resistance effects can be estimated using

$$FF = FF_0\left[1 - \frac{(v_{oc} + 0.7)}{v_{oc}}\frac{FF_0}{r_{sh}}\right] \quad [8]$$

in which $r_{sh} = R_{sh}/R_{CH}$ is the normalized shunt resistance. This equation is accurate for $v_{oc} > 10$ and $r_{sh} > 2.5$ [4]. The combined effect of series and shunt resistance can be represented by eqn [8] if FF_0 is replaced by FF as given in eqn [7]:

$$FF = FF_0(1 - r_s)\left[1 - \frac{(v_{oc} + 0.7)}{v_{oc}}\frac{FF_0(1 - r_s)}{r_{sh}}\right] \quad [9]$$

In the following, we will denote all variables as a function of irradiance level G, for example, $V_{oc}(G)$, $J_{sc}(G)$, $FF(G)$, and $\eta(G)$, while only certain variables are assumed constant.

We assume further that performance parameters V_{oc}, J_{sc}, FF, and η are available at a certain irradiance level G_0, that is, $V_{oc}(G_0)$, $J_{sc}(G_0)$, $FF(G_0)$, and $\eta(G_0)$. This level does not necessarily have to be 1000 W m^{-2}, only a known value is needed for the analysis; of course, this is usually the STC value. We further assume that the I–V characteristics can be described by an idealized one-diode model, eqn [3]. The normalized open-circuit voltage and characteristic resistance are calculated first: $v_{oc}(G_0)$ and $R_{CH}(G_0)$. Further, under the assumption that $I_L(G) = I_{sc}(G)$, the current ratio $I_L(G_0)/I_0(G_0)$ at irradiance level G_0 is calculated using eqn [3] followed by $FF_0(G_0)$ with eqn [6]. Taking into account only series resistance losses, $R_s(G_0)$ and $R_{CH}(G_0)$ are calculated using eqn [7]. Shunt resistance losses are expected to be important only at very low irradiance levels and are not included here. We further assume that both I_0 and R_s are not dependent on G. In the series resistance R_s, many components are lumped together, such as the series resistance from the metal grid, the contact resistance, and the emitter and base resistances, which generally are dependent on the injection level in the cell. However, for the sake of simplicity, we neglect irradiance dependence of R_s. Second, we assume that the short-circuit current is linearly dependent on G: $I_{sc}(G) = aG$. It is not necessary to know the constant a; we only use its linear dependence.

Figure 6 shows the results of this procedure for the c-Si cell of **Figure 2**. Comparing this method with the three-parameter fit method, it is clear that reasonable agreement is achieved over the whole range of interest down to ~50 W m^{-2}. Thus, using only STC parameters will introduce small errors in calculating annual energy yield, at least smaller errors than using a constant efficiency over the whole range [5].

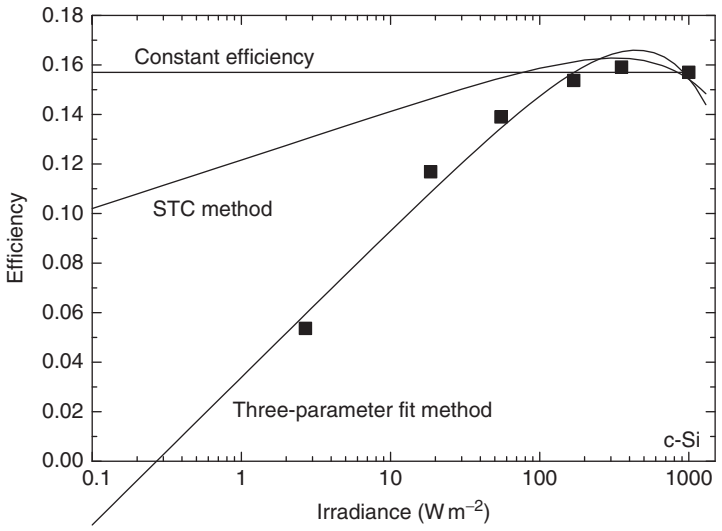

Figure 6 Efficiency of the c-Si solar cell of **Figure 2** as a function of irradiance for the three methods used; constant efficiency, three-parameter fit method, and STC method. From van Sark WGJHM (2007) Teaching the relation between solar cell efficiency and annual energy yield. *European Journal of Physics* 28: 415–427 [5].

With the method outlined above, we have calculated the irradiance-dependent behavior of the efficiency for various record efficiency cells [9, 11], see Figure 7. We have used the STC data for the 24.7% c-Si cell by University of New South Wales (UNSW), the 20.3% mc-Si cell by Fraunhofer-Institut für Solare Energiesysteme (FhG-ISE), the 9.5% a-Si:H cell by Neuchatel, the 18.8% CIGS cell by National Renewable Energy Laboratory (NREL), the 16.5% CdTe by NREL, the 10.4% dye-sensitized cell by Sharp, and the 3% polymer cell by Sharp, as reported in the 2009 record tables [11]. Clearly, all efficiencies show irradiance-dependent behavior. Some suffer from high series resistance values as evidenced from the drop in efficiency at high irradiance values.

1.32.2.1.2 Modules

Cells are assembled together in order to deliver the required currents and voltages. For example, 36 identical solar cells with characteristics as shown in Figure 2 are mounted together in series in a solar panel, see Figure 8; note that a small edge area and intercell area are present. This panel would deliver a total power of 137.5 Wp at STC at an MPP current of 7.333 A and an MPP voltage of about 17.35 V. The total cell area is 0.876 m^2. However, the panel area is larger and depends on the arrangement of the cells, for example, in a 4 by 9 way (rectangular module, Figure 8) or in a 6 by 6 way (square module). Now, using an intercell distance of 1 cm and a module edge width of 2 cm, as most modules are framed, the area of the rectangular module would be 1.058 m^2. The area of the square module is somewhat smaller at 1.053 m^2. Thus, as the area of the module is 20.7% larger than the total area of the cells, the module efficiency is 17.2% lower than the cell efficiency, which is only due to the extra needed area of the module or, in absolute terms, the 'module' efficiency is 13.0%. Using nonidentical cells, the module efficiency further suffers from mismatch loss; this is usually minimized by manufacturers by selecting cells from the same efficiency class. After cells are made, they are tested and divided into efficiency classes of 0.1% width. The above module having an efficiency of 13% is built from cells from the efficiency class 15.65–15.75%.

A 72-cell module in a 6 by 12 configuration (275.1 Wp, with the cells of Figure 2) would be 2.075 m^2 in size, with a total cell area of 1.75 m^2, leading to a panel efficiency of 13.27%. If the intercell and edge sizes are halved, the 36-cell module would have an efficiency of 14.27% and the 72-cell module 14.41%. Clearly, these 'dead' areas in the module should be minimized.

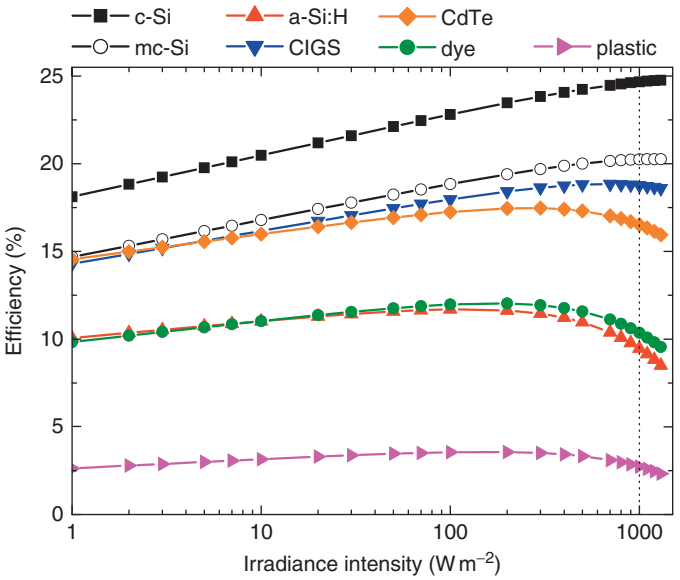

Figure 7 Efficiency of selected record efficiency solar cells [11] as a function of irradiance calculated with the STC method. Figure compiled from data presented in reference Reich NH, van Sark WGJHM, and Turkenburg WC (2011) Charge yield potential of indoor-operated solar cells incorporated into Product Integrated Photovoltaic (PIPV). *Renewable Energy* 36: 642–647 [9].

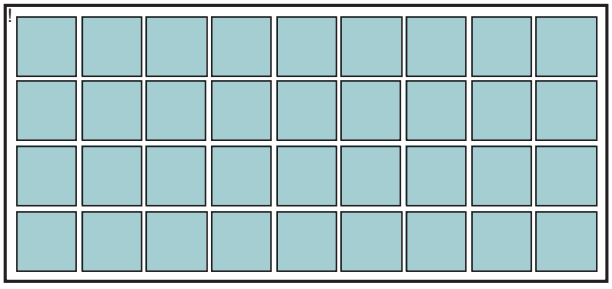

Figure 8 Schematic layout of a PV module with 36 solar cells in a 4 × 9 arrangement. Note the small but significant intercell and edge areas. From van Sark WGJHM (2007) Teaching the relation between solar cell efficiency and annual energy yield. *European Journal of Physics* 28: 415–427 [5].

Table 1 Examples of currently available PV modules

Manufacturer	*Type*	*Solar cell type*	*Rated power (Wp)*	*Short-circuit current (A)*	*Open-circuit voltage (V)*	*Size (mm × mm)*	*Cells per module*
Sunpower	SPR-327NE-WHT-D	Mono-Si	327	6.46	64.9	1559 × 1046	96
Solon	SOLON Black 280.17 (290)	Mono-Si	290	8.59	44.23	1973 × 993	72
Q-Cells	Q.Pro 250 G2	Poly-Si	250	8.58	37.72	1670 × 1000	60
Kaneka	U-EA120	a-Si	120	2.6	71	1210 × 1008	106
Sanyo	HIT-N240SE10	a-Si/c-Si	240	5.85	52.4	1580 × 798	72
Solar Frontier	SF150-L	CIS	150	2.1	110	1257 × 977	170
First Solar	FS-385	CdTe	85	1.98	61	1200 × 600	
Konarka	Power plastic 720	Thin-film organic	9.1	1.413	11.3	1553 × 340	20

Source: Photon.info module database www.photon.info/photon_site_db_solarmodule_en.photon (accessed 31 October 2011) [12].

A vast amount of different modules are or were available now or in the past. A module database maintained by Photon now lists nearly 40 000 different types of modules [12]. A few examples of current modules are listed in **Table 1**.

The present PV module market is dominated by modules made from wafer-based mono- or multicrystalline silicon at a market share of 80% [13]. Commercial monocrystalline silicon module efficiencies are between 14% and 20% and polycrystalline modules between 12% and 17%. The market share of thin-film modules presently is 16–20%, but is increasing fast [13].

1.32.3 Balance of System

1.32.3.1 Inverters

Inverters are designed to perform two main functions: (1) MPP tracking and (2) DC – AC conversion. As can be seen from **Figure 2**, the power generated by a PV cell (or module) is maximum at a certain voltage and current: the MPP. As the *I*–*V* characteristics depend on the irradiation intensity, the MPP also varies. An MPP tracker should constantly ensure that a PV module is at its MPP; this is realized by power electronic circuits, in which pulse-width modulation techniques are employed with a feedback loop to sense PV output power upon changing the voltage over the module or system until maximum power is reached [14, 15]. Here also DC–DC converters (buck–boost, boost–buck) are used: low-power inverters use metal-oxide-semiconductor field-effect transistor (MOSFET) thyristors in high-power applications, and typical efficiencies are 98% [15]. DC–AC conversion can be achieved on the basis of square wave, sine or modified sine wave, or pulse-width modulated inverters [15]. Inverter capacities may range from 500 W to 1 MW and deliver an AC output that has a waveform very close to a pure sinusoidal 50 or 60 Hz one.

Similar to PV modules, the inverter efficiency is given for its design operating power; however, the operation of inverters is usually at partial load. Therefore, it is desirable to have a high and flat efficiency curve over a wide range of partial loads.

The efficiency, η_{inv}, of the inverter is defined by

$$\eta_{\text{inv}} = \frac{P_{\text{AC}}}{P_{\text{DC}}} = \frac{P_{\text{DC}} - P_{\text{loss}}}{P_{\text{DC}}} \quad [10]$$

where P_{DC}, P_{AC}, and $P_{\text{loss}}P_{\text{DC}}$ are the instantaneous DC power, AC power, and power loss, respectively [16].

The power losses in a solar inverter consist of a constant and a load-dependent part and are not constant. As an example, **Figure 9** shows the efficiency of some inverters as a function of per unit (pu) value of the DC power [16]. The nominal power varies between 2 and 1000 kW. For all inverters, the efficiency is high and constant between 20% and 100% of the rated power. At lower levels, the efficiency decreases suddenly. Thus, for cloudy conditions, inverters with high rated powers will operate with relatively low efficiency.

In order to determine PV system performance, it is clearly necessary to take the inverter efficiency over the whole operating range into account. This is the reason for the establishment of the European inverter efficiency value η_{Euro}, which is an efficiency number weighted for the Central European climate [17]. It is defined as follows:

$$\eta_{\text{Euro}} = 0.03\eta_{5\%} + 0.06\eta_{10\%} + 0.13\eta_{20\%} + 0.1\eta_{30\%} + 0.48\eta_{50\%} + 0.2\eta_{100\%} \quad [11]$$

European efficiency values can be very high. In **Figure 10**, results from the market study in The Netherlands show that the European efficiency values depend on the size of the inverter and can be >97% for inverters larger than 5 kW [18].

A simple mathematical function has been proposed that describes the efficiency curve of any solar inverter with very good accuracy [16]:

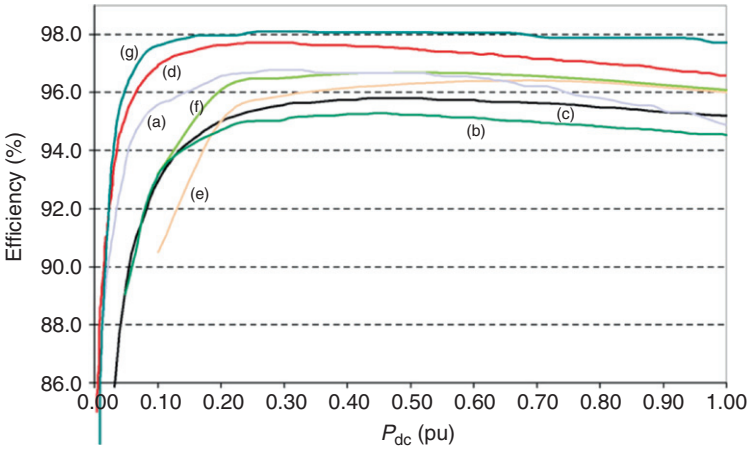

Figure 9 The efficiency of various solar inverters as a function of the pu DC power. (a) Solar Konzept, 2 kW; (b) Sunways, 3.6 kW; (c) SMA, 5 kW; (d) SMA, 11 kW; (e) Satcon, 50 kW; (f) Satcon, 100 kW; (g) Siemens, 1000 kVA. Source: Demoulias C (2010) A new simple analytical method for calculating the optimum inverter size in grid-connected PV plants. *Electric Power Systems Research* 80: 1197–1204, copyright (2010) with permission from Elsevier [16].

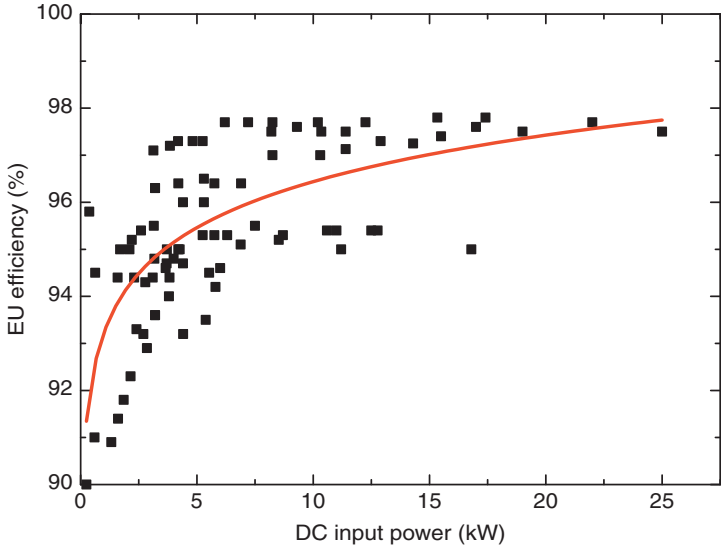

Figure 10 European efficiency of various solar inverters as a function of the DC input power. Source: Data from van Sark WGJHM, Muizebelt P, Cace J (2011) PV market in The Netherlands (in Dutch). Utrecht, The Netherlands: Stichting Monitoring Zonnestroom [18].

$$\eta_{\text{inv}}\left(P_{\text{DC,pu}}\right) = A + BP_{\text{DC,pu}} + \frac{C}{P_{\text{DC,pu}}} \quad [12]$$

in which $P_{\text{DC,pu}}$ is the pu value of the DC power. The parameters A, B, and C can be determined by fitting the curves as shown in **Figure 9**. For instance, for the Siemens 1000 kVA inverter, the parameters are $A = 98.78 \pm 0.12$, $B = -0.87 \pm 0.05$, and $C = -0.105 \pm 0.004$ [16].

When sizing a grid-connected PV system, the inverter capacity is to be matched with the PV array. Optimal PV system performance can usually be achieved by using an inverter with a capacity that is between 70% and 90% of the rating of the PV array. This obviously depends on the inverter efficiency curve and the climate characteristics.

Other requirements that utilities and standards prescribe are that acceptable levels of harmonic distortion should be achieved, that is, the voltage and current output waveforms should be of a certain quality. Further, there should be no emissions of electrical noise, as it could interfere with television or radio reception. Finally, in case of a grid failure, inverters should automatically switch off.

1.32.3.2 Mounting Structures

Mounting structures should be designed to hold the PV modules in place, and they should withstand heavy wind loads, for instance, on top of roofs as building-added PV (BAPV). For BIPV, these structures are designed to be building elements in which the PV modules are integrated. Examples are façade elements, roofing tiles, noise barriers, outdoor lighting systems, and (road) warning signs. The cost should be low, and in fact in BIPV, the cost of these elements can already be lower than marble or glazed façades. Also, mutual shading by modules should be avoided, and for maintenance, if at all necessary, easy access to the modules should be possible.

1.32.3.3 Batteries

In stand-alone systems, PV electricity is stored in rechargeable batteries; charging and discharging are regulated with the charge controller. The most commonly used battery is the lead-acid battery, although nickel-cadmium batteries are also used. Charging and discharging of batteries are unfortunately not reversible. Operation temperature and the rate of charge and discharge affect the performance and lifetime of a battery. The overall efficiency of charging and discharging is about 90% [15]. Usually slow discharge rates lead to longer lifetimes, while at low temperatures, discharge rates can decrease considerably. A sealed lead-acid battery avoids problems of spillage of the electrolyte and requires less maintenance.

1.32.3.4 Charge Regulators

Charge regulators are needed in stand-alone systems to regulate the flow of electricity between PV modules, battery, and loads. They are designed to determine the battery's state of charge (SOC) and protect the battery from overcharge or excessive discharge. PV modules operate at an approximately constant voltage under normal operating conditions, and an MPP tracker is not necessary. However, charge regulators may also contain an MPP tracker, and they use DC–DC converters to maintain a certain required system voltage; this however may be less cost-effective.

1.32.4 PV System Design

The size of a PV system may depend on the application for which it is intended. This certainly holds for stand-alone, or hybrid systems, where, for example, diesel generators are supplemented with a PV and battery system to provide electricity for remote or rural communities. For grid-connected PV systems available and suitable roof area usually determine at least the maximum size of a PV system, and cost the actual installed size. In all cases, an accurate prediction of the amount of annually generated electricity is needed to assess the feasibility of a system. The energy yield depends on the type of PV modules (i.e., their efficiency curve, as shown in **Figure 5**), the efficiency curve of the inverter (e.g., as shown in **Figure 9**), the meteorological conditions, and the orientation (south) and tilt angle of the modules. The annual energy yield nowadays can be modeled by a large selection of commercial software that differ in the level of sophistication, that is, from basic and quick assessment to full 3D simulations.

Energy losses in grid-connected PV systems that should further be taken into account are [19, 20] (1) irradiation losses such as spectral loss, reflection loss, shading loss, and soiling loss; (2) system losses such as deviating module power specifications, low irradiance losses, temperature effects, DC cable losses, various mismatch losses, static and dynamic MPP tracking losses, and inverter DC/AC and inverter control losses. Note that some of these losses are already reflected in the efficiency curves of the PV module and the inverter itself. Losses have been reduced from ~40% in the 1990s [19] to ~10% at present [20].

In the following, we present two case studies that we performed as examples of various issues that are encountered during the system design: (1) a hybrid PV–diesel system for an isolated island and (2) a large-scale PV power plant in a desert area.

1.32.4.1 Hybrid Solar–Diesel System for Mandhoo Island

A grid-connected PV–diesel hybrid system has been designed and installed at one of the outer islands of the Maldives [21]. Demonstration of a working hybrid PV–diesel system with storage backup was identified as crucial for raising awareness and building up know-how among the Maldivians. Therefore, a pilot hybrid PV–diesel system was designed for one of the islands. After reviewing a number of islands and assessing their suitability for installing such a system, the island of Mandhoo was selected. The system is expected to serve as an interesting learning experience for the Maldivians before setting up similar installations in future in other islands. In the design phase, the HOMER simulation tool has been extensively used in order to compare and optimize the electrical demand to the electrical energy that the system is able to supply on an hourly basis [22].

Mandhoo island is located about 100 km southwest of the capital Malé in the South Ari Atoll at 3′41″ N, 72′42″ E. The annual average temperature on the island is around 30 °C year-round, with a minor variation of a few degrees. The relative humidity levels are around 70–80%. The island is inhabited by about 40 families (250 persons in 2005) that are all connected to the island grid. The PV system is planned to operate in conjunction with the existing diesel power generating systems on the island, whereby the PV system in principle provides power during the day and the diesel systems during the evening and night.

The island has two diesel generators (G1 of 31 kW and G2 of 21.6 kW capacity, see **Figure 11**). Electricity is metered and sold to the households and the commercial clients at a rate (2005) of 4.5 Rf (US$ 0.35) kWh^{-1}. Another important electrical load is the streetlight in the island during nighttime. The generators are used alternately, and a manual switch is used to change the load from one to the other generator. The small diesel engine G2 runs during the day, meeting a demand that is around 6–8 kW, and the large diesel G1 is switched on around 18:00 hours to serve the peak load of about 16 kW during the evenings, with incidental peaks above 20 kW, and a nighttime demand of 12 kW. It is switched off at 06:00 hours.

Based on the gathered information, a load curve was derived. Electricity supplied by the generators amounted to 75 555 kWh in 2005, with an average of 207 kWh day^{-1}. Logged data enabled to determine the efficiency curves of both generators, as depicted in **Figure 12**. As a result, the existing system could be well-modeled using the HOMER software: electricity cost was calculated to be 0.342 US $ kWh^{-1}, using as assumptions a diesel fuel cost of 0.5 US$ l^{-1}, an interest rate of 12%, and a project lifetime of 15 years.

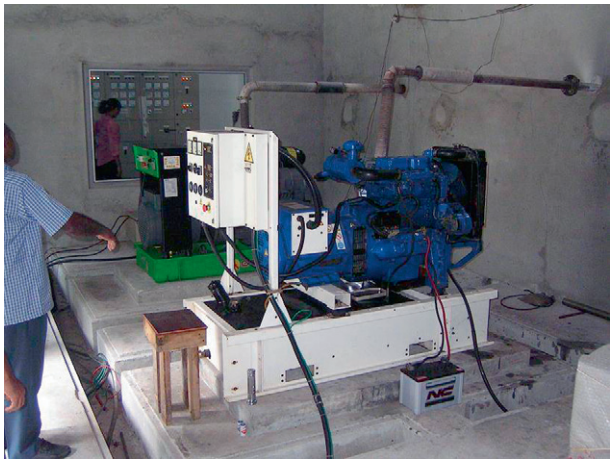

Figure 11 Existing diesel sets in Mandhoo: back 31 kW, front 22 kW. Reprinted from van Sark WGJHM, Lysen EH, Cocard D, *et al.* (2006) The first PV-diesel hybrid system in the Maldives installed at Mandhoo island. In: Poortmans J, Ossenbrink H, Dunlop E, and Helm P (eds.) *Proceedings of the 21st European Photovoltaic Solar Energy Conference*, pp. 3039–3043. Munich, Germany: WIP-Renewable Energies, with permission from WIP-Renewable Energies [21].

1.32.4.1.1 Hybrid design

1.32.4.1.1(i) Considerations

Integrating the PV system with battery backup in the current island grid was considered as a suitable way to introduce renewable electricity supply, as PV/battery systems are simply add-ons to the existing infrastructure. The system should be as simple and sturdy as possible and easy to operate for the present operator. Therefore, it was decided to go for an independent PV–battery system, that is, either the PV system or one of the diesel generators provides electricity to the distribution system. This is to be implemented through a manual switch-over between the two systems, in the same way it is being done at present, with a manual switch-over between the two diesel generators in the morning and in the evening. Synchronization was not opted for, given the added complexity and the need to add synchronization units for the diesel generators as well.

The way the operator of the power station operates the system has been integrated into the simulations of the PV–diesel system. The underlying constraints for designing the system are as follows:

- one should not expect to introduce too many changes in the operator's habits;
- both diesel generators should be turned off during a certain period of the day so that the surrounding population may feel ('hear') the difference once the PV system is installed;
- both diesel generators should be kept in operating conditions throughout the year (theoretically, one genset is sufficient to meet the load, but maintenance requires that they will be used alternatively); and
- the PV system should ideally be placed nearby the power house in order to minimize the transmission losses as well as to facilitate the maintenance of the entire system.

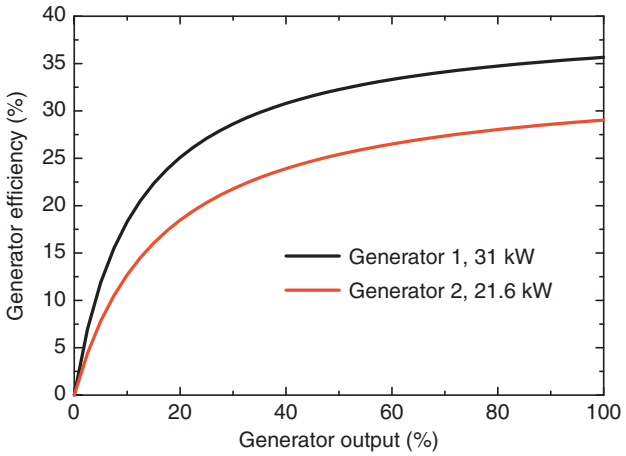

Figure 12 Generator efficiency as a function of relative output. Reprinted from van Sark WGJHM, Lysen EH, Cocard D, *et al.* (2006) The first PV-diesel hybrid system in the Maldives installed at Mandhoo island. In: Poortmans J, Ossenbrink H, Dunlop E, and Helm P (eds.) *Proceedings of the 21st European Photovoltaic Solar Energy Conference*, pp. 3039–3043. Munich, Germany: WIP-Renewable Energies, with permission from WIP-Renewable Energies [21].

The PV system should supply power to the network during daytime, from 07:00 until 18:00 hours, with the objective of avoiding the use of a diesel generator during that period and reducing the dependence on fossil fuel. As the PV system would operate during sunshine hours, the size of the storage batteries can be minimized, thus reducing the battery investment and replacement costs. On an average day, the battery will start feeding the network (through the inverter) and with higher solar radiation, the PV panel gradually takes over the load and also starts recharging the battery when extra power is available. On cloudy days, this may not be the case; then the battery will have to supply most of the load throughout the day. The HOMER model runs showed that on certain days, the battery is not able to meet the demand because it will reach a depth of discharge below 50% around midday. The operator will be instructed to switch on the diesel engines by midday on cloudy days. He will be guided by a simple indicator showing the SOC of the battery. On a normal sunny day, the operator makes a manual switch-over to one of the diesel generators at 18:00 hours. The same switch will reverse the energy flow in the converter, thereby starting to recharge the batteries. The batteries should be fully charged again before 07:00 hours of the next day. As an example of HOMER simulation results, **Figure 13** shows monthly averaged demand and supply curves.

1.32.4.1.1(ii) PV system

On the basis of local inspections and analysis with the HOMER model, the following design specifications were found to be optimal for a solar penetration of about 25%: PV capacity of 12 kWp, battery capacity of 108 kWh (50 batteries, 360 Ah, 6 V), and 12 kWp converter. The solar regime was taken from data measured (2003–05) at Hulhulé airport that is about 100 km away from Mandhoo. The average daily irradiance is 5.03 kWh m^{-2} day^{-1}, providing 1650 kWh kWp^{-1}.

In the ideal case, the PV panels should be located near the power station, but the site is not ideal as it is shaded by trees in the afternoon. Therefore, a street between the school and the health center, running from east–northeast to west–southwest, was selected. This location is partly shaded by trees, but only in the early morning and late afternoon. The PV panels are mounted on a self-standing elevated roof-like structure that is designed to withstand winds of up to 20 m s^{-1}. The structure is equipped with two gutters to lead the rain away from the edges of the panels. People are able to walk or bicycle easily below the structure.

Given the need to concentrate on the maintenance and the physical switch-over between PV and diesel generators in the powerhouse itself, it was decided to have the batteries and the converter installed in the powerhouse. This implies a long (200 m) DC connection between the PV panels and the rest of the system, which results in some DC transmission losses. The converter should be able to withstand the daily manual switch-over of the load, without voltage surges on the network.

The system was to be equipped with a monitoring system, which can be read from the Ministry of Environment, Energy and Water (MEEW) office in Malé. This is presently the case with the monitoring of weather data from three masts in the country: each data-logger sends a daily e-mail to the Malé office at 24:00 hours with the data recorded that day. In a similar manner, the monitoring system is to transmit the required 10-min average data, thus allowing to properly monitor the PV–diesel system. The monitoring system is located in the powerhouse and monitors the solar radiation (based on a global radiation pyranometer), the DC voltage and current from the PV panel to the batteries, the DC voltage and current to or from the battery bank, the DC voltage and current to or from the converter, and the outgoing AC power (three phases).

1.32.4.1.2 Realization

In a first mission to the Maldives in December 2004, the island of Mandhoo was visited and data were taken. Also, preliminary HOMER simulations were performed. During a second mission in February and March 2005, a final system design was defined together with Maldivian partners, based on acquired data of the daily load and commercially available PV and converter components. A 1-day visit to Mandhoo together with Maldivian partners marked a vital step in the introduction of the PV–diesel

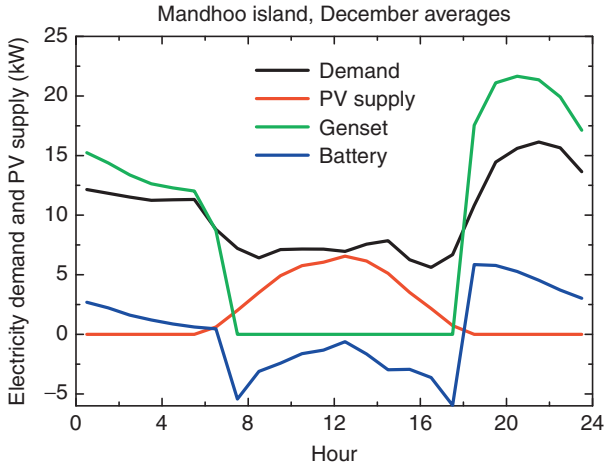

Figure 13 Daily demand and supply curves for Mandhoo in December. During this month, the PV system meets the full demand at noon, the rest being supplied by the batteries that are fully charged during night by the generator. Reprinted from van Sark WGJHM, Lysen EH, Cocard D, *et al.* (2006) The first PV-diesel hybrid system in the Maldives installed at Mandhoo island. In: Poortmans J, Ossenbrink H, Dunlop E, and Helm P (eds.) *Proceedings of the 21st European Photovoltaic Solar Energy Conference*, pp. 3039–3043. Munich, Germany: WIP-Renewable Energies, with permission from WIP-Renewable Energies [21].

Figure 14 PV system at Mandhoo. Reprinted from van Sark WGJHM, Lysen EH, Cocard D, *et al.* (2006) The first PV-diesel hybrid system in the Maldives installed at Mandhoo island. In: Poortmans J, Ossenbrink H, Dunlop E, and Helm P (eds.) *Proceedings of the 21st European Photovoltaic Solar Energy Conference*, pp. 3039–3043. Munich, Germany: WIP-Renewable Energies, with permission from WIP-Renewable Energies [21].

system in the island. The Maldivian partners had organized a meeting with all inhabitants of the island, during which a detailed presentation was made about the PV–diesel hybrid system in Dhivehi, the Maldivian language. The inhabitants unanimously voted in favor of the installation of the system.

In the months thereafter, a tender document was sent to well-known European solar system providers, inviting them to submit proposals with price quotations. Just after summer, a supplier was selected, and shipments to Malé were planned for November. In December, local workers constructed the steel support structure, and after transport of PV panels and converter to Mandhoo, installation of the PV system was carried out around Christmas and finalized on 31 December 2005. **Figure 14** shows a photograph of the finalized PV system. The structure was erected on the planned site, between the school and the Mandhoo Health Center. This will thereby serve the double purpose of providing shelter against rain or sunshine for those waiting in line for the Health Post and at the same time be of educational value for the children and teachers of the school. The installed system consists of PV capacity 12.8 kWp (160 pieces, 80 Wp. 12 V, BP), battery capacity 54 kWp (120 pieces OPzS solar 450, 450AhC120), and converter 20 kW (2 pieces, 10 kVA, Ainelec Energy Bay).

1.32.4.1.3 Evaluation

During the final mission in December 2005, it was found that the daily load of the island had substantially increased as a result of an additional air-conditioned communication center. The estimate for the daily consumption as used in the HOMER modeling exercise therefore had to be revised and was increased to 275 kWh day^{-1} (100 375 kWh yr^{-1}). Also, as the actual PV system is somewhat different from the optimum system simulated in Section 1.32.4.1.1, new HOMER runs were required. As the actual electricity consumption is expected to increase in the coming years, a few runs were made with a future value of 350 kWh day^{-1} (127 750 kWh yr^{-1}) to analyze the effect this higher consumption will have on the behavior of the PV–diesel system. Results show that in both cases, the most convenient solution for the operator is to let the generator G1 run longer in the morning, that is, until 07:00 hours for the load of 275 kWh day^{-1} or until 08:00 hours for the future load of 350 kWh day^{-1}. On cloudy days, the small generator G2 should be switched on, and this should perhaps be done every week for a few hours in order to prevent corrosion of the engine.

1.32.4.1.4 Conclusion

The first grid-connected PV system in the Maldives was successfully designed and realized. Care was taken to train MEEW employees in using the HOMER program for future developments. Also, it was found imperative to meet with the local community and to discuss the proposed system. Load curves and efficiency curves of diesel generators are indispensable in determining the most optimum configuration, as well as actual measurements of the solar regime. Finally, one has to take into account future electricity demand growth.

1.32.4.2 100 MW PV Plant in Abu Dhabi Desert Area

1.32.4.2.1 Introduction

Abu Dhabi can be identified as a place with large potential for electricity production from solar energy at competitive cost. Therefore, a study of the design of a conceptual 100 MW PV system was undertaken taking into account local climatic and geographic conditions as well as field experiences in system construction in other regions such as Germany and Spain. The focus of this study was on the economical feasibility, but also technical and environmental issues were addressed [23].

Abu Dhabi is the largest emirate of the United Arab Emirates. The emirate covers 67 340 km^2 and has a population of over 1.6 million in 2008 [24]. The Emirate of Abu Dhabi is located in the Persian Gulf and shares borders with the Kingdom of Saudi Arabia

to the west and south and Oman to the east. Desert dominates Abu Dhabi's terrain, covering over 70% of its land area, where large amounts of sunshine [25] are available for electricity generation. Rapidly increasing electricity demand and environmental pressure stimulates the thought of development of future energy demand in a sustainable way in Abu Dhabi.

The electricity sector operates on a single buyer model, with the core player Abu Dhabi Water and Electricity Company (ADWEC) buying electricity from generators and selling electricity to distribution companies. Two electricity tariff models are used: a standard and a nonstandard electricity tariff. The majority of end customers including domestic customers are connected to the low-voltage distribution network and pay a standard (flat rate) electricity tariff, which includes government subsidy. Due to variations in subsidy, different standard tariffs in the range of 3 (0.6 euroct kWh^{-1}) to 15 fils kWh^{-1} (3 euroct kWh^{-1}) result (2009 level: 1 fil = 0.2 euroct). The reason for the very low electricity tariff is that the majority of existing power generation plants run on cheap natural gas. Nevertheless, peak electricity cost can amount to 16 euroct kWh^{-1}. As rapid growth in electricity consumption is foreseen in combination with limits in natural gas supply, Abu Dhabi has high ambitions to turn itself into a global energy center that would create high-quality jobs even after its oil runs out. With new coal and oil generation plants being built – where the electricity production cost is increasing to 75 fils kWh^{-1} – solar electricity could become cost-competitive.

1.32.4.2.2 Methodology

In this study, the RETScreen Clean Energy Project Analysis Software [26] was used to facilitate processing of the collected data and perform analysis on electricity production, economics, and CO_2 emission reduction. RETScreen is based on five standard analysis processes, of which energy generation, financial analysis, and GHG emission analysis are core perspectives in our study.

The Emirate of Abu Dhabi is characterized as a subtropical climate combined with arid weather due to large imposing desert areas. The clearness index for Abu Dhabi is high, the annual average being 0.58 (varying between 0.54 and 0.65) [25, 27]. The annual average daily global horizontal solar radiation in Abu Dhabi is 5.97 kWh m^{-2} day^{-1}; average daily solar radiation at a 20° tilted plane toward the south is 6.32 kWh m^{-2} day^{-1} [27]. The monthly variation is shown in **Figure 15**, illustrating that winter and summer differences are small; this leads to a flat power generation curve throughout the year taking into account that the high temperature in summer (**Figure 15**) reduces solar conversion efficiency. Average wind speeds vary between 3 and 4 m s^{-1} (at 10 m height) over the year

Two PV technologies were selected: a wafer-based crystalline silicon (c-Si, Solarfun, 13.4% STC efficiency) and a thin-film technology (CdTe, First Solar, 10.1% STC efficiency). RETScreen calculates annual energy production using a sophisticated PV model, in which inverter and various other losses are also accounted for [26].

The conceptual 100 MW PV system is built from PV modules connected to several inverters. Depending on the specific modules (c-Si and CdTe) and inverters, a specific yield can be expected. A system layout is shown in **Figure 16**. The 100 MW PV plant consists of 100 subsystems of 1 MW each. Each subsystem converts DC electricity from two 500 kW PV arrays to 20 kV AC electricity through a SMA Sunny Central 1000 MV medium voltage station [28], which contains two identical high-efficiency inverters and a medium voltage transformer. In the case of c-Si modules, we integrated 196 subsystems into the 100 MW PV plant, with each pair connected to a Sunny Central 1000 MV substation. The Sunny Central 1000 MV substation (colored pink in **Figure 16**) is located in between each 1.02 MW subsystem in order to minimize wiring distance and complexity. The Sunny Central 1000 MV substation converts DC electricity from the 1.02 MW solar field to AC electricity with medium voltage of 20 kV, which then is fed into the 220 kV transmission grid through a 20 kV/220 kV transformer. The entire system demands an area of 1.65 km^2 and consists of 100 Sunny Central 1000 MV stations and 501 760 c-Si modules of 200 Wp. For CdTe modules of 72.5 Wp each, in total 1 380 000 modules are used in 200 sets of 500.25 kWp array units each. The total area is 2.09 km^2.

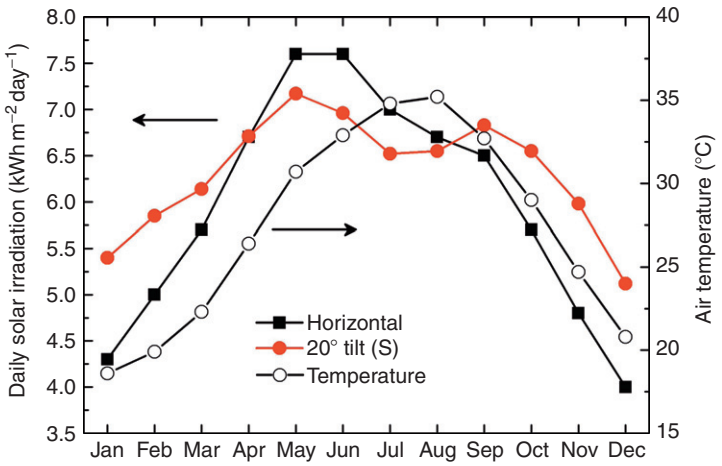

Figure 15 Monthly variation of daily solar irradiation in the horizontal plane and for a 20° tilted plane toward the south (left axis). Monthly variation of air temperature (right axis). Reprinted from Zhang C, van Sark WGJHM, and van Schalkwijk M (2010) Technical configuration, economic feasibility and environmental impacts of a 100 MW solar PV plant in desert areas in the Abu Dhabi Emirate. In: Sayigh A (ed.) *Proceedings of the World Renewable Energy Congress XI*, pp. 1056–1061. Brighton, UK: WREN, with permission from WREN [23].

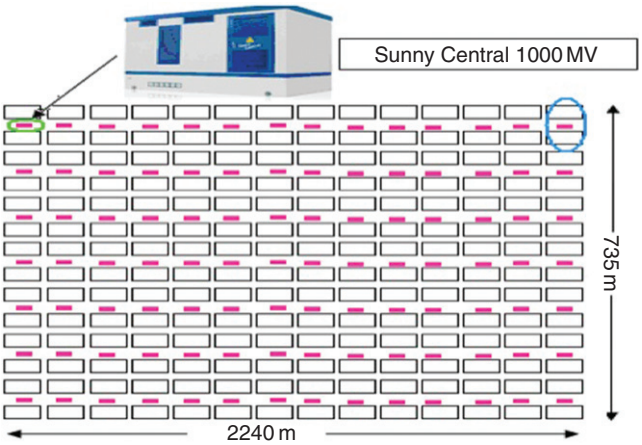

Figure 16 PV system layout. Reprinted from Zhang C, van Sark WGJHM, and van Schalkwijk M (2010) Technical configuration, economic feasibility and environmental impacts of a 100 MW solar PV plant in desert areas in the Abu Dhabi Emirate. In: Sayigh A (ed.) *Proceedings of the World Renewable Energy Congress XI*, pp. 1056–1061. Brighton, UK: WREN, with permission from WREN [23].

The profitability is determined using cost–benefit analysis; both net present value (NPV) and the payback period (PBP) are calculated. The simple PBP follows from dividing the initial investment (I) by the annual net benefit (B–C). Alternatively, the internal rate of return (IRR) reveals the discount rate at which the NPV is equal to zero.

1.32.4.2.3 Scenarios

In this study, three scenarios are established to compare economic feasibility of the 100 MW PV plant. Common parameters are inflation and discount rate, both at 10%, a project lifetime of 25 years, and a debt ratio of 70% at a debt period of 20 years at 10% interest. 'Scenario 1' presumes that feed-in-tariff (FiT) schemes similar to those in Germany are established by the Abu Dhabi government in order to accelerate deployment of renewable energy, cope with climate change, and create new economic growth sectors apart from the oil sector. The FiT rate is set fixed at 300 euro MWh^{-1} for a large-scale ground-based solar PV plant and remains constant for 25 years. Under 'scenario 2', the assumption is made based on increasing stress on shortage of natural gas supply. In this case, many gas-based generation plants are retrofitted to oil-based plants. The consequence is a sharp jump in generation cost from less than 20 to 75 fils kWh^{-1}. In these circumstances, electricity generated by PV plant is sold at a peak rate of 75 fils kWh^{-1} (150 euro MWh^{-1}) at the first year of generation. From year 1 on, an annual decrease of 10% is adopted. 'Scenario 3' takes into account the possibility of water production coupled with electricity production of the PV plant. Despite the low (mainly winter) precipitation of 100 mm each year in the deserts of Abu Dhabi, a large volume of rainwater collection is possible taking into account the potential rainwater catchment area of about 0.7 (c-Si) or 0.9 (CdTe) km^2. Using a project lifetime of 25 years and a rainwater efficiency of 75%, 52.5 million liters rainwater can be collected for c-Si (for CdTe 67.5 million liters).

1.32.4.2.4 Assumptions

The initial cost of the 100 MW plant was estimated on combining 1 MW blocks at costs regularly encountered in Spain (for systems designed in 2009). Module and support structure cost is assumed similar, and inverter cost is based on a quotation from SMA. Construction cost is adapted to local level, while engineering and training cost is 20% larger due to lack of experience in Abu Dhabi. In summary, the total initial cost for the 100 MW PV plant based on c-Si modules was 376.5 million euro, of which 56% is spent on modules. Total initial cost for the 100 MW PV plant based on CdTe modules was 360 million euro, of which 48% is spent on modules. The operation and maintenance (O&M) cost is estimated by averaging a few reported values in the range of 0.084–0.22% of the initial cost [8, 9], resulting in 0.11% of initial cost for the c-Si case and 0.12% for the CdTe case.

Regarding environmental impact of the 100 MW PV plant in Abu Dhabi, the focus was on greenhouse gas emissions (GHGs) determined by life cycle analysis (LCA) and the energy payback time (EPBT), using data of existing studies [29]. The LCA GHG emissions are 30–45 and 19–25 g CO_2 equiv. kWh^{-1} for c-Si and CdTe, respectively. Using corrections considering module efficiency, cell thickness, system performance, and electricity mix, we found a GHG emission factor for the used c-Si (CdTe) modules of 422 (59) kg CO_2 equiv. m^{-2} and a cumulative energy consumption of 3813 (1070) MJ m^{-2}. For the BOS (inverter, support structures, and cabling), these values are 17 (18) kg CO_2 equiv. m^{-2} and 543 (647) MJ m^{-2}, respectively.

1.32.4.2.5 System performance

Running the RETScreen energy model yields the following results. The 100 MW PV plant will deliver 177 GWh electricity annually for the c-Si case and 182 GWh electricity for the CdTe case without considering module degradation. The capacity factor for the c-Si case is 20.2% and a slightly higher value of 20.8% is found for the CdTe case. Finally, a performance ratio of 76.8% is calculated for the c-Si case and 79.0% for the CdTe case.

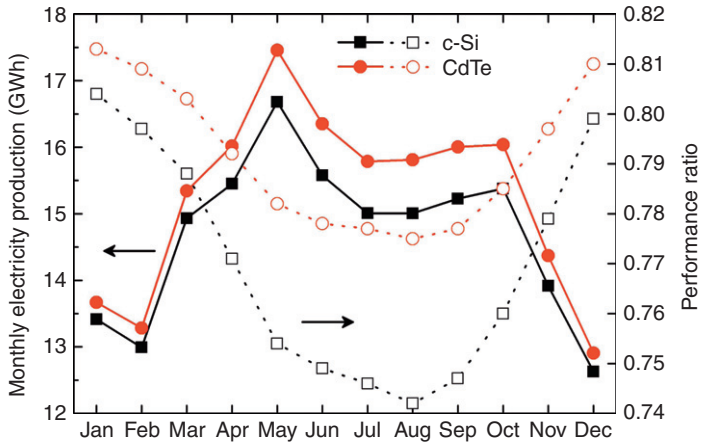

Figure 17 Monthly electricity production and performance ratio for c-Si and CdTe modules. Reprinted from Zhang C, van Sark WGJHM, and van Schalkwijk M (2010) Technical configuration, economic feasibility and environmental impacts of a 100 MW solar PV plant in desert areas in the Abu Dhabi Emirate. In: Sayigh A (ed.) *Proceedings of the World Renewable Energy Congress XI*, pp. 1056–1061. Brighton, UK: WREN, with permission from WREN [23].

Monthly electricity output is shown in Figure 17. For both technology cases, maximum electricity production occurs in May (16.7 GWh for c-Si and 17.5 GWh for CdTe) and minimum electricity production occurs in December (15.0 GWh for c-Si and 15.8 GWh for CdTe) when the solar radiation is at the lowest point. Despite the low performance ratio due to increasing temperature from June to September, more electricity is produced in summer, which matches very well with peak power demand due to substantial cooling load in those hot months. The highest performance ratio in both cases occurs in January: 80.4% for c-Si and 81.3% for CdTe. Due to high temperatures in August, the performance ratio decreases to a minimum: 74.3% for c-Si and 77.5% for CdTe.

For the calculation of total generated amount of electricity over the whole lifetime, we assumed that 90% power output at the end of 10 years and 80% power output at the end of 25 years lifetime is guaranteed. The calculated lifetime electricity output for the c-Si plant amounts to 3932 GWh, that is, 157.3 GWh on average per year. For the CdTe plant, the total electricity output is predicted to be 4047 GWh, that is, 161.9 GWh on average per year.

1.32.4.2.6 Financial results

Table 2 summarizes the general financial results of the three scenarios for both the c-Si and the CdSe technology cases. With constant FiT of 300 euro MWh^{-1} for 25 years assumed under scenario 1, the PV plant is economically attractive, with high IRR and low equity payback time (5 years) for both technologies. Electricity production costs for c-Si are 276.2 euro MWh^{-1} (257.2 euro MWh^{-1} for CdTe). The NPV of the c-Si project is about 35 million euro. For CdTe, the NPV is nearly double that of c-Si at 65.2 million euro. For both technologies, scenario 2 shows better IRR and NPV. A different approach is used under scenario 3 to calculate rainwater net profit rate in order to meet minimum cutoff IRR of a company, that is, 12% in our case. Therefore, the results only show minimum requirement for a project to be considered. Under this scenario, the electricity is sold at a tariff of 150 euro MWh^{-1}, constant for 25 years. Bottled rainwater is collected from the solar plant and sold with a net profit of 17 euroct l^{-1}, with consideration of 10% inflation rate. Under these assumptions, the IRR on company's equity is 12.3% (c-Si) and 12.7% (CdTe). Electricity production cost stands at 125.3 (c-Si) and 124.1 euro MWh^{-1} (CdTe). Equity payback time is 11.2 (c-Si) and 10.6 years (CdTe). B–C ratio and debt payback capacity are fairly low.

Figure 18 shows yearly cumulative cash flow throughout the lifetime of the PV plant under the three scenarios for both technologies, showing that technology differences are small. For c-Si, in scenario 1, positive cash flow starts before year 6.

Table 2 Summary of financial results for both technologies and the three scenarios used, compiled from data in reference 23

	c-Si technology			*CdTe technology*		
Financial viability	*Scenario 1*	*Scenario 2*	*Scenario 3*	*Scenario 1*	*Scenario 2*	*Scenario 3*
After-tax IRR – equity (%)	14.9	16.8	12.3	19.2	18.4	12.7
Equity payback (years)	5.7	9.8	11.2	4.7	8.8	10.6
NPV (million euro)	35.2	168.9	36.5	65.2	202.9	39.4
Benefit–cost (B–C) ratio	1.3	2.5	1.3	1.6	2.9	1.4
Debt service coverage	1.7	0.9	1.2	1.8	1.0	1.2
Energy production cost (euro MWh^{-1})	276.2	106.1	125.3	257.2	99.3	124.1

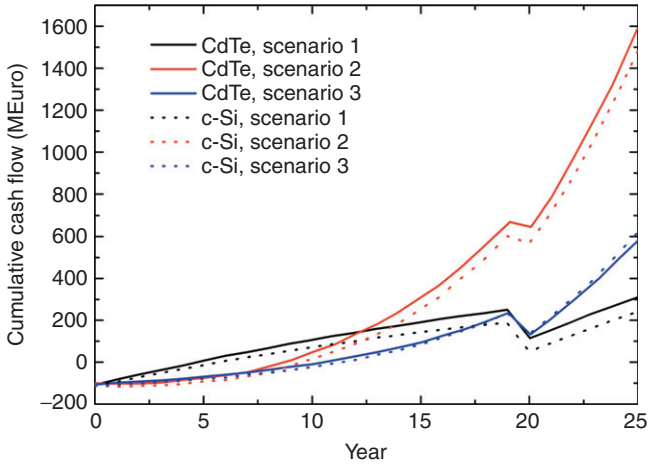

Figure 18 Cumulative cash flow under three scenarios for c-Si (dotted lines) and CdTe (solid lines). Reprinted from Zhang C, van Sark WGJHM, and van Schalkwijk M (2010) Technical configuration, economic feasibility and environmental impacts of a 100 MW solar PV plant in desert areas in the Abu Dhabi Emirate. In: Sayigh A (ed.) *Proceedings of the World Renewable Energy Congress XI*, pp. 1056–1061. Brighton, UK: WREN, with permission from WREN [23].

Periodic costs take place in year 20 due to replacement of inverters, which explains the sharp drop in year 20. End-of-life cumulative cash flow peaks at about 250 million euro. Yearly cash flow is nearly tripled after year 20 when the debt is paid up. In case of scenario 2, positive cash flow starts much later compared with scenario 1 due to the fact that electricity export rate is low at the early phase of the project and escalates gradually. Periodic costs take place in year 20 because of replacement of inverters, but the cost is less compared with substantial cash inflows cumulated in the later phase of the project. End-of-life cumulative cash flow peaks at about 1500 million euro. In scenario 3, positive cash flow happens after year 11. Periodic costs take place in year 20 because of replacement of inverters, which covers a big proportion of cumulative cash in that year. End-of-life cumulative cash flow peaks at about 620 million euro. For CdTe, similar observations can be made.

1.32.4.2.7 Environmental results

In our study, we conducted a rough estimation of GHG emission and EPBT of the conceptual PV plant. Input values are taken from the available literature with correction to some extent. From our rough estimation of GHG emissions and EPBT, we find that the potential for GHG emission reduction is significant. It is possible to reduce GHG emissions by 64 653 t yr^{-1} if c-Si modules are used; 76 983 t yr^{-1} for CdTe. Since the production process of CdTe modules is less energy-intensive than that of c-Si, the EPBT is 1.2 years for CdTe and 2.35 years for c-Si.

1.32.4.2.8 Conclusions

From this study [23], it was concluded that solar PV technology is very promising in Abu Dhabi. A 100 MW PV project can deliver substantial electricity for meeting the peak electricity demand locally and make some contribution to relieve cooling load stress in the summer season. However, as the current electricity tariff is low, financial incentives are needed. An FiT of 150 euro MWh^{-1} (scenario 2) would be economically viable. Note that this study was performed in 2009; since then, PV module prices have been decreased by >50%. Together with an expected increase of the peak electricity tariff to 15 ct kWh^{-1}, deployment of PV may be attractive with a low or even without a financial incentive.

The low cost of CdTe modules, their increasing efficiency, less energy-intensive production process, and the extreme hot climate in Abu Dhabi cause CdTe modules to be the best choice in terms of energetic performance, economic viability, and environmental impact, irrespective of the scenario considered.

1.32.5 Conclusions

In this chapter, various PV system components are described, with a focus on their individual performance. In grid-connected systems, PV modules are connected to the inverter, which converts DC PV power to AC, which is fed directly into the grid. In properly designed stand-alone systems, an additional charge controller and battery ensure that power is available at all times. PV module efficiency depends on the solar irradiation intensity and on temperature, and different types of modules differ in their specific efficiency behavior. Similarly, inverter efficiency depends on the percentage of maximum capacity at which they are operated. PV system design should include both PV and inverter efficiency curves and also other system losses. Finally, two case study examples are presented that show more details of the PV system design.

References

[1] Eltawil MA and Zhao Z (2010) Grid-connected photovoltaic power systems: Technical and potential problems – A review. *Renewable and Sustainable Energy Reviews* 14: 112–129.

[2] Komoto K, Ito M, van der Vleuten P, *et al.* (eds.) (2009) *Very Large Scale Photovoltaic Systems: Socio-Economic, Financial, Technical and Environmental Aspects*. London, UK: Earthscan.

[3] Nieuwenhout FDJ, van Dijk A, Lasschuit PE, *et al.* (2001) Experience with solar home systems in developing countries: A review. *Progress in Photovoltaics: Research and Applications* 9: 455–474.

[4] Green MA (1982) *Solar Cells; Operating Principles Technology and Systems Application*. Englewood Cliffs, NJ: Prentice-Hall.

[5] van Sark WGJHM (2007) Teaching the relation between solar cell efficiency and annual energy yield. *European Journal of Physics* 28: 415–427.

[6] Marion B (2002) A method for modeling the current-voltage curve of a PV module for outdoor conditions. *Progress in Photovoltaics: Research and Applications* 10: 205–214.

[7] Grunov P, Lust S, Sauter D, *et al.* (2004) Weak light performance and annual energy yields of PV modules and systems as a result of the basic parameter set of industrial solar cells. In: Hoffmann W, Bal J-L, Ossenbrink H, *et al.* (eds.) *Proceedings of the Nineteenth European Photovoltaic Solar Energy Conference*, pp. 2190–2193. Munich, Germany: WIP.

[8] Reich NH, van Sark WGJHM, Alsema EA, *et al.* (2009) Crystalline silicon cell performance at low light intensities. *Solar Energy Materials & Solar Cells* 93: 1471–1481.

[9] Reich NH, van Sark WGJHM, and Turkenburg WC (2011) Charge yield potential of indoor-operated solar cells incorporated into Product Integrated Photovoltaic (PIPV). *Renewable Energy* 36: 642–647.

[10] Beyer HG, Betcke J, Drews A, *et al.* (2004) Identification of a general model for the MPP performance of PV-modules for the application in a procedure for the performance check of grid connected systems. In: Hoffmann W, Bal J-L, Ossenbrink H, *et al.* (eds.) *Proceedings of the 19th European Photovoltaic Solar Energy Conference*, pp. 3073–3076. Munich, Germany: WIP.

[11] Green MA, Emery K, King DL, *et al.* (2009) Solar cell efficiency tables (version 33). *Progress in Photovoltaics: Research and Applications* 17: 85–94.

[12] Photon.info Module Database www.photon.info/photon_site_db_solarmodule_en.photon (accessed 31 October 2011).

[13] Jäger-Waldau A (2011) PV Status Report 2011. Research, Solar Cell Production and Market Implementation of Photovoltaics, European Commission, DG Joint Research Centre, Institute for Energy, Renewable Energy Unit.

[14] Krauter S (2006) *Solar Electric Power Generation-Photovoltaic Energy Systems*. Berlin, Germany: Springer-Verlag.

[15] Messenger RA and Ventre J (2010) *Photovoltaic Systems Engineering*, 3rd edn. New York: CRC Press.

[16] Demoulias C (2010) A new simple analytical method for calculating the optimum inverter size in grid-connected PV plants. *Electric Power Systems Research* 80: 1197–1204.

[17] Bletterie B, Bründlinger R, and Lauss G (2011) On the characterisation of PV inverters' efficiency – Introduction to the concept of achievable efficiency. *Progress in Photovoltaics: Research and Applications* 19: 423–435.

[18] van Sark WGJHM, Muizebelt P, and Cace J (2011) PV market in The Netherlands (in Dutch). Utrecht, The Netherlands: Stichting Monitoring Zonnestroom.

[19] Reinders AHME, van Dijk VAP, Wiemken E, and Turkenburg WC (1999) Technical and economic analysis of grid-connected PV systems by means of simulation. *Progress in Photovoltaics: Research and Applications* 7: 71–82.

[20] Reich NH, Mueller B, Armbruster A, *et al.* (2012) Performance ratio revisited: Are PR > 90% realistic? *Progress in Photovoltaics* 20 (in press).

[21] van Sark WGJHM, Lysen EH, Cocard D, *et al.* (2006) The first PV-diesel hybrid system in the Maldives installed at Mandhoo island. In: Poortmans J, Ossenbrink H, Dunlop E, and Helm P (eds.) *Proceedings of the 21st European Photovoltaic Solar Energy Conference*, pp. 3039–3043. Munich, Germany: WIP-Renewable Energies.

[22] Lambert T, Gilman P, and Lilienthal P (2006) Micropower system modeling with HOMER. In: Farret FA and Simões MG (eds.) *Integration of Alternative Sources of Energy*, pp. 379–418. New York: Wiley.

[23] Zhang C, van Sark WGJHM, and van Schalkwijk M (2010) Technical configuration, economic feasibility and environmental impacts of a 100 MW solar PV plant in desert areas in the Abu Dhabi Emirate. In: Sayigh A (ed.) *Proceedings of the World Renewable Energy Congress XI*, pp. 1056–1061. Brighton, UK: WREN.

[24] Abu Dhabi Tourism Authority http://www.visitabudhabi.ae/en/about.abudhabi.aspx (accessed 23 February 2012).

[25] Islam MD, Kubo I, Ohadi M, and Alili AA (2009) Measurement of solar energy radiation in Abu Dhabi, UAE. *Applied Energy* 86: 511–515.

[26] Natural Resources Canada (2005) *Clean Energy Project Analysis-RETScreen® Engineering & Cases Textbook*. http://www.retscreen.net. (accessed 23 February 2012).

[27] NASA Surface Meteorology and Solar Energy Data Set http://eosweb.larc.nasa.gov/sse/. (accessed 23 February 2012).

[28] SMA Solar Technology http://www.sma.de (accessed 23 February 2012).

[29] Fthenakis V and Alsema EA (2006) Photovoltaics energy payback times, greenhouse gas emissions and external costs: 2004–early 2005 status. *Progress in Photovoltaics* 14: 275–280.